

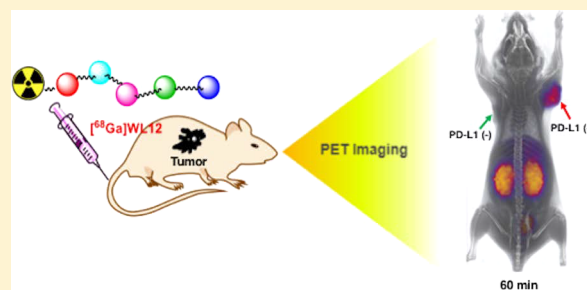
Peptide-Based ^{68}Ga -PET Radiotracer for Imaging PD-L1 Expression in Cancer

Ravindra A. De Silva,¹ Dhiraj Kumar, Ala Lisok, Samit Chatterjee, Bryan Wharram, Kalagadda Venkateswara Rao, Ronnie Mease, Robert F. Dannals, Martin G. Pomper,¹ and Sridhar Nimmagadda*

Russell H. Morgan Department of Radiology and Radiological Science, Sidney Kimmel Comprehensive Cancer Center, Johns Hopkins University, Baltimore, Maryland 21287, United States

ABSTRACT: Tumors create and maintain an immunosuppressive microenvironment that promotes cancer cell escape from immune surveillance. The immune checkpoint protein programmed death-ligand 1 (PD-L1) is expressed in many cancers and is an important contributor to the maintenance of the immunosuppressive tumor microenvironment. PD-L1 is a prominent target for cancer immunotherapy. Guidance of anti-PD-L1 therapy is currently effected through measurement of PD-L1 through biopsy and immunohistochemistry. Here, we report a peptide-based imaging agent, [^{68}Ga]WL12, to detect PD-L1 expression in tumors noninvasively by positron emission tomography (PET). WL12, a cyclic peptide comprising 14 amino acids, binds to PD-L1 with high affinity ($\text{IC}_{50} \approx 23 \text{ nM}$). Synthesis of [^{68}Ga]WL12 provided radiochemical purity >99% after purification. Biodistribution in immunocompetent mice demonstrated 11.56 ± 3.18 , 4.97 ± 0.8 , 1.9 ± 0.1 , and 1.33 ± 0.21 percentage of injected dose per gram (%ID/g) in hPD-L1, MDAMB231, SUM149, and CHO tumors, respectively, at 1 h postinjection, with high binding specificity noted with coinjection of excess, nonradiolabeled WL12. PET imaging demonstrated high tissue contrast in all tumor models tested.

KEYWORDS: PD-1, NSCLC, peptide, TNBC, immune checkpoint therapy



INTRODUCTION

Immuno-oncology is revolutionizing cancer therapy by producing durable responses that lead to improved survival of patients with a variety of malignancies. The immune checkpoint protein programmed death ligand 1 (PD-L1) is one important target of those therapeutic efforts. PD-L1 is expressed in many tumors as an immune evasion mechanism.¹ Measurement of PD-L1 through biopsy and immunohistochemistry (IHC) is used to select patients for therapy and for therapeutic monitoring in those undergoing anti-PD-L1 axis treatment.^{2,3} However, PD-L1 IHC has significant limitations, including conflicting results between different detection antibodies, insufficient interassay agreement, and heterogeneity in PD-L1 expression within and across tumor sites.⁴ Also, PD-L1 expression in the tumors is temporally dynamic, and these changes are difficult to capture during therapy as repeat biopsy is often impractical.⁵ Those issues are compounded in patients with advanced stage disease, a population in which immune checkpoint inhibitors are currently investigated. Noninvasive quantification of total PD-L1 expression in all lesions concurrently could address some of those limitations and assist in therapeutic decision-making.

Noninvasive imaging technologies such as positron emission tomography (PET) can provide quantitative, real-time assessment of target expression and dynamics that enable therapeutic monitoring.^{6,7} We and others have demonstrated the potential

of radiolabeled anti-PD-L1 antibodies, nanobodies, and small proteins to image PD-L1 expression in different tumor models.^{8–14} In spite of those promising developments, the relatively longer biological half-lives of radiolabeled antibodies in clinical trials necessitate a wait period of 4 to 7 days to get high tissue contrast.¹⁵ This could potentially delay a switch to alternative treatment. Thus, for rapid and accurate imaging of PD-L1 dynamic changes during treatment, novel probes with shorter biological half-lives are needed. Such probes provide opportunities to better select patients in relatively shorter periods of time early during treatment. Specially, small peptide and low-molecular-weight imaging agents often exhibit faster pharmacokinetics (minutes to hours) than small proteins and antibodies (hours to days), and produce high-contrast images within a clinically useful time frame. Not surprisingly, most routinely used clinical radiopharmaceuticals, particularly for PET, are either peptides or low-molecular-weight agents.¹⁶

High-affinity peptide-based PD-L1 inhibitors have recently been reported.¹⁷ The pharmacokinetics of those peptides, however, have not been matched with routinely used PET radionuclides such as ^{68}Ga or ^{18}F . Our recently reported cyclic

Received: April 16, 2018

Revised: July 3, 2018

Accepted: July 23, 2018

Published: July 23, 2018

14-amino-acid peptide, its 1,4,7,10-tetraazacyclododecane,1-(glutaric acid)-4,7,10-triacetic acid (DOTAGA) conjugate (WL12), and copper-chelated analogs ($[^{64}\text{Cu}]\text{WL12}$) demonstrated high in vitro PD-L1 binding affinity ($\text{IC}_{50} = 2.9 \text{ nM}$ for the metalated version) and in vivo specific tumor targeting ability.¹⁸ With the promising results observed using $[^{64}\text{Cu}]\text{WL12}$, our attention has turned to generating a similar compound radiolabeled with ^{68}Ga . Interest for ^{68}Ga for imaging applications comes from its ready availability from a generator, its routine use in many clinical centers, and the 67.6 min half-life of ^{68}Ga , which results in low radiation exposure. Also, ^{68}Ga half-life matches well with the pharmacokinetic properties of peptides. Additionally, kit type preparation similar to that of $^{99\text{m}}\text{Tc}$ is feasible. Recently clinical applications of ^{68}Ga -based radiotracers have been increasing,^{19–23} with several ^{68}Ga -radiolabeled agents in widespread clinical use.^{24–29} For example, $[^{68}\text{Ga}]\text{DOTA}-(\text{Tyr}3)\text{-octreotate}$ (DOTATATE) is largely replacing the time-honored standard for imaging neuroendocrine tumors, $[^{111}\text{In}]\text{octreotide}$, for detection of neuroendocrine tumors.

A PD-L1-targeted imaging agent that leverages the benefits of ^{68}Ga for PET has not been reported. The rapid normal tissue clearance observed with WL12 is optimal for the short physical half-life of ^{68}Ga .¹⁸ Accordingly, we have developed $[^{68}\text{Ga}]\text{WL12}$ as a PD-L1 imaging agent. Here, we report a radiosynthetic procedure designed to generate highly pure $[^{68}\text{Ga}]\text{WL12}$ that is easily scalable to clinical studies. Biodistribution and PET imaging studies demonstrate PD-L1 specificity of $[^{68}\text{Ga}]\text{WL12}$ in multiple tumor models with variable PD-L1 expression. $[^{68}\text{Ga}]\text{WL12}$ can be used to quantify PD-L1 expression in tumors and may be useful shortly after administration in clinical studies, enabling seamless integration into standard clinical workflow.

■ EXPERIMENTAL SECTION

Materials. WL12 was custom synthesized by CPC Scientific (Sunnyvale, CA) with >95% purity and 2,2',2''-(10-(2,6-dioxotetrahydro-2H-pyran-3-yl)-1,4,7,10-tetraazacyclododecane-1,4,7-triyl) triacetic acid (DOTAGA anhydride) was purchased from CheMatech Macrocycle Design Technologies (catalog #C109; Dijon, France). All other chemicals were purchased from Sigma-Aldrich or Fisher Scientific unless otherwise specified. Eckert and Ziegler $^{68}\text{Ge}/^{68}\text{Ga}$ -generator was used as a ^{68}Ga source, and ^{68}Ga was eluted using 0.5 N HCl solution. TraceSELECT grade water and sodium acetate were used for ^{68}Ga labeling. All cell culture related reagents were purchased from Invitrogen.

Synthesis of DOTAGA Conjugated PD-L1 Binding Peptide (WL12). DOTAGA conjugated WL12 was synthesized and characterized according to our previously published procedure.¹⁸ Briefly, to a solution of WL12 (3 mg, 1.5 μmol) and diisopropylethylamine (20.0 μL , 0.2 μmol) in 1.0 mL of dimethylformamide (DMF) was added DOTAGA anhydride (3.7 mg, 7.51 μmol), and the reaction mixture was stirred for 2 h at room temperature. The reaction mixture was purified on a reversed phase high performance liquid chromatography (RP-HPLC) system using a semipreparative C-18 Luna column (5 μm , 10 \times 250 mm, Phenomenex, Torrance, CA). The HPLC column was eluted with (A) methanol (0.1% TFA) and (B) water (0.1% TFA) using a linear gradient from 2/98 (A/B) to 100/0 (A/B) over 60 min at a flow rate of 4 mL/min. The desired DOTAGA conjugated WL12 was collected at 44.5 min, solvent evaporated, residue dissolved in deionized water,

and lyophilized to form a solid product. The purified WL12-DOTAGA was characterized by electrospray ionization mass spectroscopy.

Radiolabeling and Purification of $[^{68}\text{Ga}]\text{WL12}$. A fractionation method was used for ^{68}Ga elution. The generator was eluted with 0.5 N HCl solution,³⁰ the first fraction (1.0 mL) was discarded, and the next fraction (2.0 mL) containing >85% of radioactivity was transferred into a reaction vial containing WL12 peptide (30 μg) and 0.5 N sodium acetate buffer (600 μL , pH 4.5). The pH of the final reaction was 3.5–4.0. ^{68}Ga radiolabeling was performed without stirring at 100 $^{\circ}\text{C}$ for 10 min. After completion, a sample ($\sim 20 \mu\text{L}$) was analyzed for radiochemical purity by RP-HPLC. The cooled crude reaction mixture was passed through a preconditioned C-18 Sep-Pak cartridge, rinsed with 10 mL of ultrapure water, and eluted with 1.0 mL of ethanol. Preconditioning of the cartridge was performed with 5 mL of methanol followed by 10 mL of water. The radiochemical purity of Sep-Pak purified $[^{68}\text{Ga}]\text{WL12}$ was assessed by RP-HPLC. A semipreparative C-18 Luna column (5 μm , 10 \times 250 mm Phenomenex, Torrance, CA) with (A) methanol (0.1% TFA) and (B) water (0.1% TFA) using a linear gradient from 60/40 (A/B) to 90/10 (A/B) over 30 min at a flow rate of 5 mL/min was used for peak separation. For in vitro and in vivo evaluation, ethanol was evaporated and $[^{68}\text{Ga}]\text{WL12}$ was formulated in saline containing 5% DMSO and two drops of Tween 20.

Cell Lines. Chinese hamster ovary cell line CHO-K1 (CHO) and triple negative breast cancer (TNBC) cell line MDAMB231 were purchased from the American Type Culture Collection (ATCC, Manassas, VA) and passaged for fewer than 3 months after which new cultures were initiated from vials of frozen cells. All other cell lines were cultured in ATCC recommended media in an incubator at 37 $^{\circ}\text{C}$ in an atmosphere containing 5% CO_2 . CHO cell line stably expressing human PD-L1 (hPD-L1) was generated in our laboratory¹⁰ and maintained in F-12K medium with 10% FBS, 1% P/S, and 2 mg/mL G418. The SUM149 cell line was kindly provided by Dr. Stephen P. Ethier, Medical University of South Carolina, and authenticated by STR profiling at JHU. SUM149 cells were maintained in Ham's F-12 medium with 5% FBS, 1% P/S, 5 mg/mL insulin, and 0.5 mg/mL hydrocortisone.

Flow Cytometry Analysis for PD-L1 Expression in Cell Lines. Surface PD-L1 expression levels were analyzed using an anti-human PD-L1 antibody conjugated with phycoerythrin (BD-MIH1-PE, clone # MIH1, catalog #557924) according to procedures described previously.¹⁸

Immunohistochemistry. Tumor sections were evaluated for PD-L1 expression by immunohistochemistry (IHC). Harvested tumors were fixed in 10% neutral buffered formalin and embedded in paraffin, and 4 μm thick sections were obtained on slides. After deparaffinizing with xylene and alcohol gradients, antigen retrieval was done using 10 mM citrate buffer, pH 6.0 (#S1699, Dako target retrieval solution). Tumor sections were then treated with 3% H_2O_2 for 10 min, blocked with 5% goat serum for 1 h, and then incubated with a primary antihuman PD-L1 antibody (#13684, Cell Signaling) at 1:500 dilution at 4 $^{\circ}\text{C}$ overnight. Subsequently, using Dako CSAII Biotinfree Tyramide Signal Amplification System kit, slides were incubated with secondary antibody, amplification reagent and with antfluorecein-HRP. Finally, staining was carried out by adding DAB chromogen. Sections were counterstained with hematoxylin, followed by dehydration

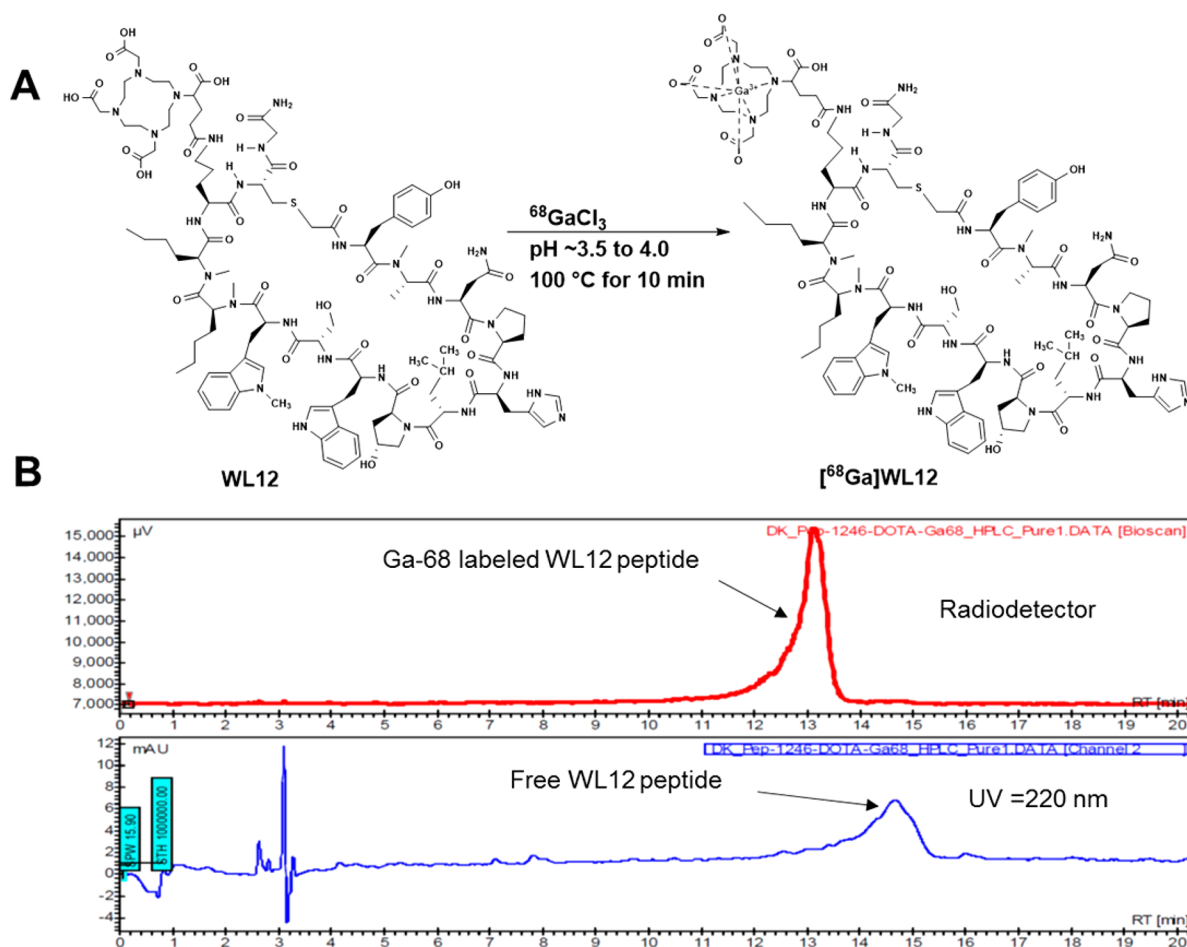


Figure 1. WL12 radiolabeling conditions and radiochemical purity of $[^{68}\text{Ga}]\text{WL12}$. WL12 was radiolabeled with $^{68}\text{GaCl}_3$ at $100\text{ }^\circ\text{C}$ for 10 min at $\text{pH} \approx 3.5$ to 4.0 and purified by C-18 Sep-Pak. (A) $[^{68}\text{Ga}]\text{WL12}$ structure and labeling conditions. (B) RP-HPLC chromatograms of purified $[^{68}\text{Ga}]\text{WL12}$.

with alcohol gradients, xylene washes, and mounted with a coverslip.

Animal Models. Animal studies were performed according to the protocols approved by the JHU Animal Care and Use Committee using six-to-eight-week-old, female, nonobese diabetic severe-combined immunodeficient gamma (NSG) mice obtained from the JHU Immune Compromised Animal Core. Mice were implanted subcutaneously in opposite sides of the upper flanks with 10×10^6 of hPD-L1 and CHO cells or with MDAMB231 and SUM149 cells (5×10^6 cells). Mice were used for imaging or biodistribution when the tumor sizes reached volumes of 200–500 mm^3 .

PET-CT Imaging. Mice were injected with $\sim 74 \times 10^5$ Bq (200 μCi) of $[^{68}\text{Ga}]\text{WL12}$ intravenously, anesthetized under 3% isoflurane prior to being placed on the scanner. PET images were acquired in two bed positions at 10 min/bed in an ARGUS small-animal PET-CT scanner (Sedecal, Madrid, Spain) as described previously.¹⁴ For hPD-L1 and CHO tumor bearing mice ($n = 3$), the whole-body PET images were acquired at 15, 60, and 120 min after injection of radiotracer. For MDAMB231 and SUM149 tumor models ($n = 3$), mice were imaged at 60 min after $[^{68}\text{Ga}]\text{WL12}$ injection. To establish the in vivo specificity, mice were subcutaneously administered with a blocking dose of WL12 (50 μg) 60 min before injection of $[^{68}\text{Ga}]\text{WL12}$.

Ex Vivo Biodistribution. NSG mice harboring hPD-L1, CHO, SUM149, and MDAMB231 tumors ($n = 3$) were injected intravenously with 9.25×10^5 Bq (25 μCi) of $[^{68}\text{Ga}]\text{WL12}$. The biodistribution studies were performed according to the procedure described previously.¹⁸ For the mice with hPD-L1 and CHO tumors, the studies were performed at 15, 60, and 120 min, and for the mice with SUM149 and MDAMB231 tumors, the data was collected at 60 min time point. For specificity studies, a separate group of mice bearing tumors ($n = 2$) were subcutaneously administered with a 50 μg blocking dose of WL12 at 60 min before the injection of $[^{68}\text{Ga}]\text{WL12}$. The %ID/g values were calculated based on signal decay correction and normalization to external $[^{68}\text{Ga}]$ standards, which were measured in triplicate. Biodistribution data shown is mean \pm standard error of the mean (SEM).

Data Analysis. Statistical analysis was performed using the Prism 6 Software (GraphPad Software, La Jolla, CA). P -values < 0.05 were considered to be significant using an unpaired two tailed t test, and the comparative reference was cell line or tumor with low PD-L1 expression. Molinspiration software was used to calculate the partition coefficient value (LogP) of $[^{68}\text{Ga}]\text{WL12}$.³¹

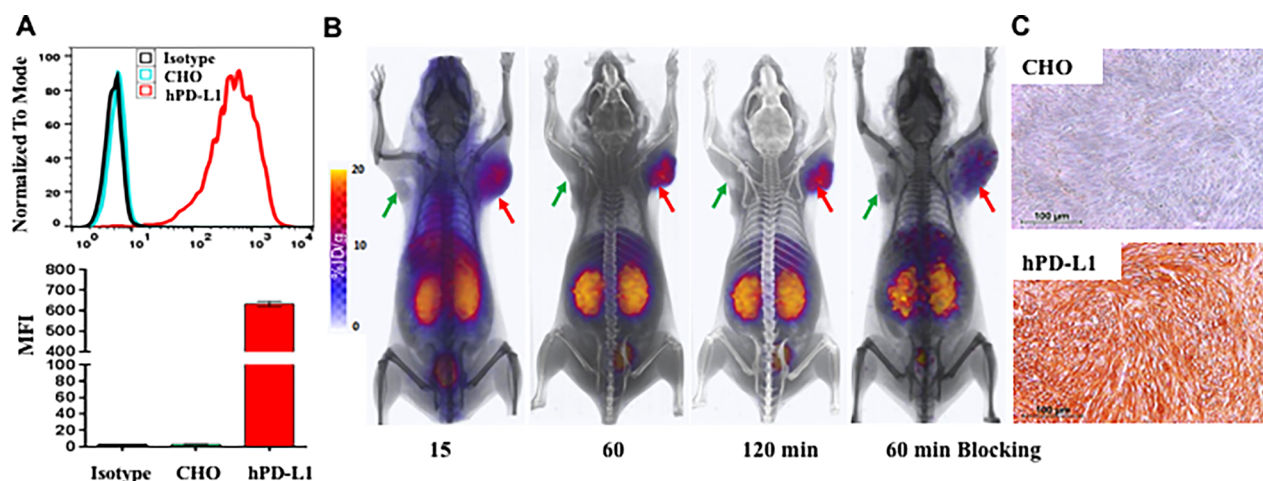


Figure 2. Evaluation of [^{68}Ga]WL12 in hPD-L1 and CHO tumor models. (A) Flow cytometry shows higher PD-L1 expression in hPD-L1 cells compared to that in the CHO cell line (black, isotype; green, CHO cell line; red, hPD-L1 cell line). (B) PET-CT images of [^{68}Ga]WL12 uptake in hPD-L1 (red arrow, high PD-L1 expression) and CHO (green arrow, low PD-L1 expression) tumors confirm PD-L1-mediated uptake of the radiotracer. (C) Immunohistochemical analysis for PD-L1 expression demonstrating high immunoreactivity in hPD-L1 tumors (brown) compared to that in CHO tumors (purple).

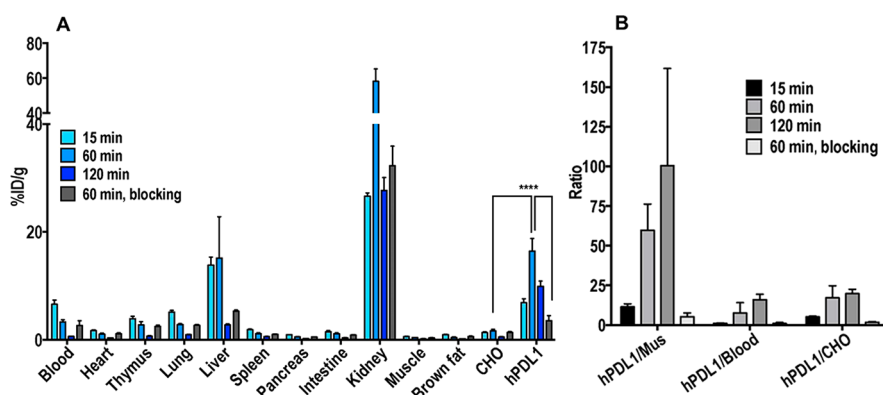


Figure 3. Ex vivo evaluation of [^{68}Ga]WL12 in hPD-L1 and CHO tumor models. (A) Ex vivo biodistribution analysis of [^{68}Ga]WL12 at 15 min, 60 min, 120 min ($n = 3$), and 60 min blocking ($n = 2$) after injection in the same tumor models; ****, $p \leq 0.0001$. (B) Analysis of tumor to blood and tumor to muscle ratios of [^{68}Ga]WL12 uptakes.

RESULTS AND DISCUSSION

Synthesis and Characterization of ^{68}Ga Radiolabeling of WL12.

Lyophilized WL12 was collected as a white powder in good chemical yield (3.0 mg, 80.0%). The observed mass from ESI-MS was m/z : $2402.6 - (M + 1)^+$, $1201.9 - (M + 2)^{+2}/2$ (Expected: 2402.18). The synthesis of [^{68}Ga]WL12, including C-18 Sep-Pak purification, was completed within 20 min. Radio-HPLC assessment of the crude product showed >95% radiochemical purity. C-18 Sep-Pak purification resulted in >99% pure [^{68}Ga]WL12 (Figure 1A). Our ^{68}Ga generator was one year old and yielded approximately 3.7×10^7 Bq (1 mCi) activity to start with; however, the synthesis procedures used consistently yielded $80 \pm 5\%$ (decay corrected) radiochemically pure [^{68}Ga]WL12 and with a low specific activity of 128 GBq/ μmol . The labeling and purification methods we have tested here can be easily modified to develop a kit-based preparation of [^{68}Ga]WL12. The calculated partition coefficient (LogP) value for [^{68}Ga]WL12 by Molinspiration software is -5.99 (octanol–water partition coefficient).^{31,32} An excellent agreement between experimental LogP and Molinspiration calculated LogP was reported by National Institute of Standards and Technology.³³

In Vivo Kinetics, Distribution, and Specificity of [^{68}Ga]WL12 in Human Programmed Cell Death Ligand 1 (hPD-L1) and CHO Tumor Model.

Mice bearing hPD-L1 and CHO tumors were tested to determine the in vivo kinetics and distribution of [^{68}Ga]WL12. Flow cytometry analysis confirmed the high PD-L1 expression in hPD-L1 cells compared to that of control CHO cells (Figure 2A). The mean fluorescence intensity (MFI) values for hPD-L1 and CHO cells were approximately 600 and 10, respectively (Figure 2A). The PET-CT images of hPD-L1/CHO mice showed significantly higher accumulation of [^{68}Ga]WL12 in hPD-L1 tumors (Figure 2B, red arrows) compared to control CHO tumors (Figure 2B, green arrows). Uptake of [^{68}Ga]WL12 could be observed in hPD-L1 tumors as early as 15 min and retained through 120 min postinjection indicating PD-L1 specificity (Figure 2B). The specificity of [^{68}Ga]WL12 was further confirmed in a blocking study. The PET images of mice receiving preinjection of excess nonradioactive WL12 showed a significant reduction of [^{68}Ga]WL12 uptake in hPD-L1 tumors confirming that [^{68}Ga]WL12 uptake in the tumor is PD-L1 specific. In addition to tumors, high uptake was observed in kidneys that are involved in excretion of the tracer. High uptake was also observed in the liver (Figure 2B).

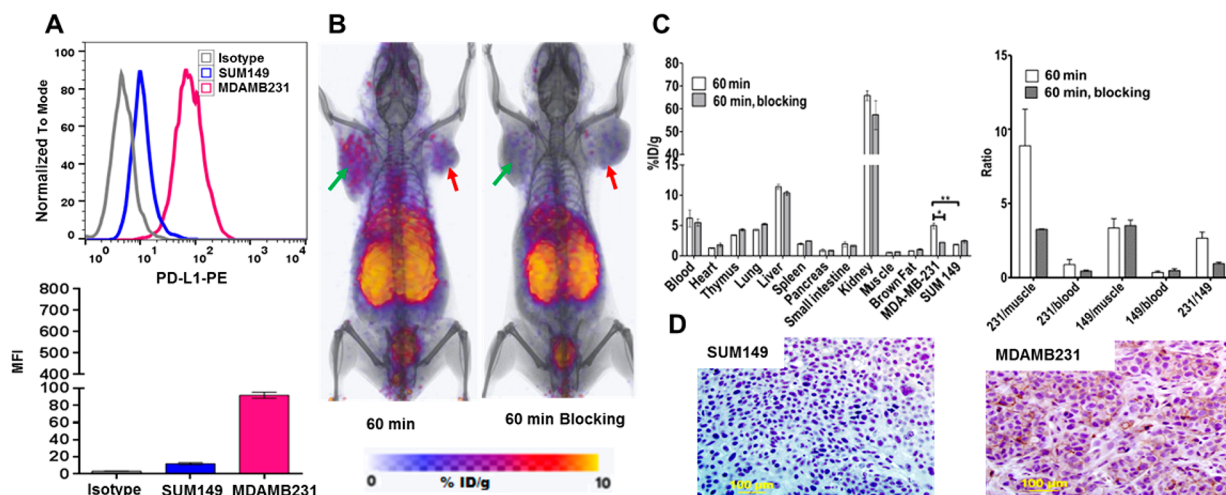


Figure 4. Evaluation of $[^{68}\text{Ga}]\text{WL12}$ in MDAMB231 and SUM 149 tumor models. (A) Flow cytometry shows higher PD-L1 expression in MDAMB231 cells compared to that in the SUM149 cell line (black, isotype; blue, SUM149 cell line; red, MDAMB231 cell line). (B) PET-CT images of $[^{68}\text{Ga}]\text{WL12}$ uptake in MDAMB231 (green arrow, high PD-L1 expression) and SUM 149 (red arrow, low PD-L1 expression) tumors confirm PD-L1-mediated uptake of the radiotracer. (C) Ex vivo biodistribution analysis of $[^{68}\text{Ga}]\text{WL12}$ at 60 min ($n = 3$) and 60 min blocking ($n = 2$) after injection in the same tumor models; * $p \leq 0.05$, ** $p \leq 0.01$. (D) Immunohistochemical analysis for PD-L1 expression demonstrating high immunoreactivity in MDAMB231 tumors (purple) compared to that in SUM149 tumors (blue).

To validate our PET imaging observations, biodistribution studies were performed at 15, 60, and 120 min time points (Figure 3). Biodistribution studies showed greater than 9-fold increase of $[^{68}\text{Ga}]\text{WL12}$ accumulation in hPD-L1 tumors at all the time points tested, compared to control CHO tumors (Figure 3A). The percentage of injected dose per gram of tissue (%ID/g) for hPD-L1 tumors was 19.4 ± 3.3 , 11.56 ± 3.18 , and 9.89 ± 1.72 at 15, 60, and 120 min after injection, respectively. In contrast, control CHO control tumors showed $<1.33 \pm 0.21$ uptake of $[^{68}\text{Ga}]\text{WL12}$ at the same time points. The PD-L1-mediated uptake of $[^{68}\text{Ga}]\text{WL12}$ in hPD-L1 tumors was further confirmed by reduced uptake of radioactivity observed in the blocking experiment. In blocking dose mice, approximately 75% decrease in the uptake of radioactivity in hPD-L1 tumors (5.1 ± 0.2) was observed at 60 min compared to mice that did not receive the blocking dose.

The high PD-L1 specific accumulation of $[^{68}\text{Ga}]\text{WL12}$ in PD-L1 positive tumors resulted in tumor-to-muscle ratios of 59.79 ± 16.47 and 100.47 ± 61.23 at 60 and 120 min, respectively. The tumor-to-blood ratios of 7.56 ± 16.47 and 16.02 ± 3.40 at 60 and 120 min, respectively, showed fast clearance of the tracer from circulation. The imaging and biodistribution results were consistent with IHC data that showed intense PD-L1 immunoreactivity in hPD-L1 tumors and not in control CHO tumors (Figure 2C).

$[^{68}\text{Ga}]\text{WL12}$ showed better image contrast at 60 and 120 min after administration compared to $[^{64}\text{Cu}]\text{WL12}$.¹⁸ The blood %ID/g values at 60 and 120 min were 3.3 ± 0.4 and 0.6 ± 0.01 for $[^{68}\text{Ga}]\text{WL12}$ and 3.6 ± 1.0 and 3.3 ± 0.1 for $[^{64}\text{Cu}]\text{WL12}$, respectively. Radiotracer uptake was similar for both the analogs in the hPD-L1 tumors at 60 min ($\sim 16\%$ ID/g). A 40% decreased in $[^{68}\text{Ga}]\text{WL12}$ uptake was observed in hPD-L1 tumors at 120 min compared to $[^{64}\text{Cu}]\text{WL12}$, a reflection of increased clearance observed with $[^{68}\text{Ga}]\text{WL12}$.

Differences were also observed in normal tissue uptake, with $[^{68}\text{Ga}]\text{WL12}$ exhibiting less liver and muscle uptake than $[^{64}\text{Cu}]\text{WL12}$.¹⁸ The uptake of $[^{68}\text{Ga}]\text{WL12}$ in the liver was 50–90% less than that observed with $[^{64}\text{Cu}]\text{WL12}$. Liver uptake for $[^{68}\text{Ga}]\text{WL12}$ was 15.1 ± 7.6 and $2.7 \pm 0.2\%$ ID/g at

60 and 120 min, respectively, and for $[^{64}\text{Cu}]\text{WL12}$, it was 34.3 ± 3.1 and $24.2 \pm 2.5\%$, respectively, at the same time points. Differences were also observed in kidney uptake. The kidney uptake (%ID/g) for $[^{68}\text{Ga}]\text{WL12}$ at 60 min was 64.7 ± 12.1 and rapidly reduced to 27.67 ± 4.09 at 120 min, whereas kidney uptake of $[^{64}\text{Cu}]\text{WL12}$ was 34.3 ± 3.1 and $27.7 \pm 2.7\%$ ID/g at 60 and 120 min, respectively. Taken together, these data indicate faster clearance of $[^{68}\text{Ga}]\text{WL12}$ that results in high contrast images. Supporting those observations, the hPD-L1 tumor-to-muscle and hPD-L1 tumor-to-blood ratios at 120 min were 100.47 ± 61.23 and 16.02 ± 3.40 , respectively, for $[^{68}\text{Ga}]\text{WL12}$ vs 25.65 ± 1.9 and 4.7 ± 1.2 , respectively, for $[^{64}\text{Cu}]\text{WL12}$. Faster clearance of $[^{68}\text{Ga}]\text{WL12}$ also resulted in improved hPD-L1/CHO tumor ratios of 19.7 ± 2.7 vs 3.9 ± 0.6 for $[^{64}\text{Cu}]\text{WL12}$ at 120 min.

Transchelation of ^{64}Cu , a commonly observed phenomena with ^{64}Cu imaging agents, could be a contributing factor to the low contrast observed with $[^{64}\text{Cu}]\text{WL12}$. The higher kidney uptake of $[^{68}\text{Ga}]\text{WL12}$ (%ID/g = $64.7\% \pm 12.1$) could be due to renal clearance, a trend generally observed with small peptides.³⁴ $[^{68}\text{Ga}]\text{WL12}$ image contrast could be further improved with the coadministration of lysine, or a mixture of similar positively charged amino acids, to reduce kidney accumulation of radioactivity.³⁴ Those strategies were also shown to be effective in reducing radiotoxicity associated with renal clearance.³⁴ Taken together, these results demonstrate that $[^{68}\text{Ga}]\text{WL12}$ provides suitable contrast for rapid imaging of PD-L1 expression and dynamics in tumors.

Radiolabeled antibodies, PD-1 derived fragments and adnectin derived small proteins (~ 10 kDa), have been reported for PD-L1 detection in contrast to our small peptides (2 kDa).^{8–10,12,13,35} All those agents provide PD-L1 specific images albeit requiring longer clearance times that span days to hours in contrast to our small peptides that require <60 min. Additionally, the advantage of small peptides and the potential to modify their biodistribution was evident in the different pharmacokinetics and image contrast shown by $[^{64}\text{Cu}]\text{WL12}$ and $[^{68}\text{Ga}]\text{WL12}$. ^{68}Ga -labeled peptide, due to increased hydrophilicity, shows improved image contrast. It would be

difficult to manipulate the pharmacokinetics of small proteins in a similar fashion. Also, manufacturing of biologicals is more complex, costly, time-consuming and challenging than chemically based peptides. Advancement of a radiolabeled biopharmaceutical adds an extra layer of complexity and logistical challenges compared to small molecules and peptides.

Validation of PD-L1 Specificity of [⁶⁸Ga]WL12 in MDAMB231 and SUM149 TNBC Model. We next validated [⁶⁸Ga]WL12 to detect PD-L1 expression in mice with MDAMB231 and SUM149 TNBC xenografts. PD-L1 binding peptides have not been investigated in tumor models with endogenous PD-L1 expression and to detect PD-L1 expression in multiple tumor models with variable PD-L1 expression. MDAMB231 cells have endogenously increased PD-L1 expression, which is similar to that observed in patients' tumors. Flow cytometry analysis showed that MDAMB231 and SUM149 cells exhibit high and low endogenous PD-L1 expression (Figure 4A), with the MFI values of 90 and 15, respectively. These results show that PD-L1 expression in MDAMB231 cells is roughly 7-fold lower than that of hPD-L1 cells, thus providing an opportunity to test the potential of [⁶⁸Ga]WL12 to detect variable PD-L1 expression in the tumors.

Considering the high image contrast observed with [⁶⁸Ga]-WL12 in hPD-L1 tumor model at 60 min, we conducted PET imaging and biodistribution studies at 60 min. The PET-CT images of MDAMB231/SUM149 tumor-bearing mice ($n = 3$) showed significantly high uptake of [⁶⁸Ga]WL12 in MDAMB231 tumors, compared to SUM149 (Figure 4B). The high uptake observed in MDAMB231 tumors was reduced in mice receiving blocking dose, further confirming the PD-L1 specificity of [⁶⁸Ga]WL12. Ex vivo biodistribution studies also validated the imaging study results. The [⁶⁸Ga]WL12 uptake in MDAMB231 and SUM149 tumors was 4.97 ± 0.8 and $1.9 \pm 0.1\%$ ID/g ($P < 0.01$) at 60 min, respectively (Figure 4C). [⁶⁸Ga]WL12 uptake in MDAMB231 tumors is significantly higher than both control tumors (SUM149 and CHO) and lower than the hPD-L1 tumors that have nearly 7-fold high PD-L1 expression. These results validate that [⁶⁸Ga]WL12 has the potential to detect variable PD-L1 expression levels in the tumors. Blocking dose of WL12 resulted in >50% reduction in [⁶⁸Ga]WL12 uptake in MDAMB231 tumors. Because in vivo studies were performed sequentially in these tumor models, we speculate that low specific activity and nonspecific uptake associated with the agent may have contributed to the differences in normal tissue uptake. No significant difference in uptake was observed in SUM149 tumors or any other tissues in blocking dose mice, underlining the specificity of [⁶⁸Ga]-WL12 for human PD-L1. IHC analysis of the collected tumors for PD-L1 expression showed intense immunoreactivity in MDAMB231 tumors (Figure 4D) but not in SUM149 xenografts, further validating flow cytometry, imaging, and biodistribution results. Normal tissue distribution observed in breast tumor model was similar to that observed in hPD-L1/CHO tumor model, with kidney ($65.6 \pm 3.6\%$ ID/g) and liver ($11.4 \pm 0.7\%$ ID/g) showing high radioactivity accumulation. Taken together, our results establish that [⁶⁸Ga]WL12 is capable of detecting variable PD-L1 expression levels in the tumors with high specificity.

The ultimate proof of an imaging agent specificity to its target is characterized by in vivo experiments such as PET imaging and biodistribution studies. Our in vivo PET imaging and biodistribution studies in four different tumor models

clearly demonstrate the high PD-L1 binding specificity of [⁶⁸Ga]WL12. Although a change of metal from copper to gallium could alter the binding affinity, the almost identical hPD-L1 tumor uptake at 60 min indicates similar affinity. Because emphasis of our study is to evaluate the in vivo pharmacokinetics of the agent, we have focused on comparing the in vivo distribution and kinetics of [⁶⁸Ga]WL12 and [⁶⁴Cu]WL12.

CONCLUSION

We demonstrated the specificity of [⁶⁸Ga]WL12 to detect PD-L1 expression in multiple xenograft models with variable PD-L1 expression and described its biodistribution and pharmacokinetics. In addition, the radiolabeling and purification conditions tested for preparation of [⁶⁸Ga]WL12 can be easily modified to facilitate a kit preparation of the radiotracer for PD-L1 imaging. Such ⁶⁸Ga labeled PD-L1 imaging agents with short biological half-life and fit within the routine clinical work flow can enable therapy monitoring and stratification of patients in the field of immuno-oncology and globally without the necessity for accelerators.

AUTHOR INFORMATION

Corresponding Author

*Fax: (+1) 410-614-3147. E-mail: snimmag1@jhmi.edu.

ORCID

Ravindra A. De Silva: 0000-0002-7858-5542

Martin G. Pomper: 0000-0001-6753-3010

Notes

The authors declare no competing financial interest.

ACKNOWLEDGMENTS

This work was supported by Allegheny Health Network—Johns Hopkins Cancer Research Fund, NIH R01CA16631, NIH P30 CA006973, R01CA236616, and P41 EB024495. We thank Dr. Polina Sysa-Shah for help in acquiring the PET images.

REFERENCES

- (1) He, J.; Hu, Y.; Hu, M.; Li, B. Development of PD-1/PD-L1 Pathway in Tumor Immune Microenvironment and Treatment for Non-Small Cell Lung Cancer. *Sci. Rep.* **2015**, *5*, 13110.
- (2) Teng, M. W.; Ngiow, S. F.; Ribas, A.; Smyth, M. J. Classifying Cancers Based on T-cell Infiltration and PD-L1. *Cancer Res.* **2015**, *75* (11), 2139–45.
- (3) Dolled-Filhart, M.; Roach, C.; Toland, G.; Stanforth, D.; Jansson, M.; Lubiniecki, G. M.; Ponto, G.; Emancipator, K. Development of a Companion Diagnostic for Pembrolizumab in Non-Small Cell Lung Cancer Using Immunohistochemistry for Programmed Death Ligand-1. *Arch. Pathol. Lab. Med.* **2016**, *140*, 1243.
- (4) Meng, X.; Huang, Z.; Teng, F.; Xing, L.; Yu, J. Predictive biomarkers in PD-1/PD-L1 checkpoint blockade immunotherapy. *Cancer Treat. Rev.* **2015**, *41* (10), 868–76.
- (5) Taube, J. M.; Anders, R. A.; Young, G. D.; Xu, H.; Sharma, R.; McMiller, T. L.; Chen, S.; Klein, A. P.; Pardoll, D. M.; Topalian, S. L.; Chen, L. Colocalization of inflammatory response with B7-h1 expression in human melanocytic lesions supports an adaptive resistance mechanism of immune escape. *Sci. Transl. Med.* **2012**, *4* (127), 127ra37.
- (6) Willmann, J. K.; van Bruggen, N.; Dinkelborg, L. M.; Gambhir, S. S. Molecular imaging in drug development. *Nat. Rev. Drug Discovery* **2008**, *7* (7), 591–607.

- (7) Kobayashi, H.; Longmire, M. R.; Ogawa, M.; Choyke, P. L.; Kawamoto, S. Multiplexed imaging in cancer diagnosis: applications and future advances. *Lancet Oncol.* **2010**, *11* (6), 589–95.
- (8) Heskamp, S.; Hobo, W.; Molkenboer-Kuening, J. D.; Olive, D.; Oyen, W. J.; Dolstra, H.; Boerman, O. C. Noninvasive Imaging of Tumor PD-L1 Expression Using Radiolabeled Anti-PD-L1 Antibodies. *Cancer Res.* **2015**, *75* (14), 2928–36.
- (9) Maute, R. L.; Gordon, S. R.; Mayer, A. T.; McCracken, M. N.; Natarajan, A.; Ring, N. G.; Kimura, R.; Tsai, J. M.; Manglik, A.; Kruse, A. C.; Gambhir, S. S.; Weissman, I. L.; Ring, A. M. Engineering high-affinity PD-1 variants for optimized immunotherapy and immuno-PET imaging. *Proc. Natl. Acad. Sci. U. S. A.* **2015**, *112* (47), E6506–14.
- (10) Chatterjee, S.; Lesniak, W. G.; Gabrielson, M.; Lisok, A.; Wharram, B.; Sysa-Shah, P.; Azad, B. B.; Pomper, M. G.; Nimmagadda, S. A humanized antibody for imaging immune checkpoint ligand PD-L1 expression in tumors. *Oncotarget* **2016**, *7* (9), 10215–27.
- (11) Natarajan, A.; Mayer, A. T.; Reeves, R. E.; Nagamine, C. M.; Gambhir, S. S. Development of Novel ImmunoPET Tracers to Image Human PD-1 Checkpoint Expression on Tumor-Infiltrating Lymphocytes in a Humanized Mouse Model. *Molecular imaging and biology: MIB: the official publication of the Academy of Molecular Imaging* **2017**, *19*, 903.
- (12) Hettich, M.; Braun, F.; Bartholoma, M. D.; Schirmbeck, R.; Niedermann, G. High-Resolution PET Imaging with Therapeutic Antibody-based PD-1/PD-L1 Checkpoint Tracers. *Theranostics* **2016**, *6* (10), 1629–40.
- (13) Josefsson, A.; Nedrow, J. R.; Park, S.; Banerjee, S. R.; Rittenbach, A.; Jammes, F.; Tsui, B.; Sgouros, G. Imaging, Biodistribution, and Dosimetry of Radionuclide-Labeled PD-L1 Antibody in an Immunocompetent Mouse Model of Breast Cancer. *Cancer Res.* **2016**, *76* (2), 472–9.
- (14) Lesniak, W. G.; Chatterjee, S.; Gabrielson, M.; Lisok, A.; Wharram, B.; Pomper, M. G.; Nimmagadda, S. PD-L1 Detection in Tumors Using [(64)Cu]Atezolizumab with PET. *Bioconjugate Chem.* **2016**, *27* (9), 2103–10.
- (15) Wang, G. X.; Guo, L. Q.; Gainor, J. F.; Fintelman, F. J. Immune Checkpoint Inhibitors in Lung Cancer: Imaging Considerations. *AJR, Am. J. Roentgenol.* **2017**, *209* (3), 567–575.
- (16) Sun, X.; Li, Y.; Liu, T.; Li, Z.; Zhang, X.; Chen, X. Peptide-based imaging agents for cancer detection. *Adv. Drug Delivery Rev.* **2016**, *110–111*, 38.
- (17) Miller, M. M.; Mapelli, C.; Allen, M. P.; Bowsher, M. S.; Gillis, E. P.; Langley, D. R.; Mull, E.; Poirier, M. A.; Sanghvi, N.; Sun, L.-Q.; Tenney, D. J.; Yeung, K.-S.; Zhu, J.; Gillman, K. W.; Zhao, Q.; Grant-Young, K. A.; Scola, P. M. Macrocyclic inhibitors of the PD1/PDL1 and CD80 (B7-1)/PD-L1 protein/protein interactions. WO2016039749A1, 2016.
- (18) Chatterjee, S.; Lesniak, W. G.; Miller, M. S.; Lisok, A.; Sikorska, E.; Wharram, B.; Kumar, D.; Gabrielson, M.; Pomper, M. G.; Gabelli, S. B.; Nimmagadda, S. Rapid PD-L1 detection in tumors with PET using a highly specific peptide. *Biochem. Biophys. Res. Commun.* **2017**, *483* (1), 258–263.
- (19) Banerjee, S. R.; Pomper, M. G. Clinical applications of Gallium-68. *Appl. Radiat. Isot.* **2013**, *76*, 2–13.
- (20) Martiniova, L.; De Palatis, L.; Etchebehere, E.; Ravizzini, G. Gallium-68 in Medical Imaging. *Curr. Radiopharm.* **2016**, *9*, 187.
- (21) Prata, M. I. Gallium-68: a new trend in PET radiopharmacy. *Curr. Radiopharm.* **2012**, *5* (2), 142–9.
- (22) Velikyan, I. 68Ga-based radiopharmaceuticals: production and application relationship. *Molecules* **2015**, *20* (7), 12913–12943.
- (23) Tworowska, I.; Ranganathan, D.; Thama, S.; Delpassand, E.; Mojtahedi, A.; Schultz, M. K.; Zherosekov, K.; Marx, S. Radiosynthesis of clinical doses of 68Ga-DOTATATE (GalioMedix) and validation of organic-matrix-based 68Ge/68Ga generators. *Nucl. Med. Biol.* **2016**, *43* (1), 19–26.
- (24) Giovacchini, G.; Giovannini, E.; Riondato, M.; Ciarmiello, A. PET/CT WITH 68Ga-PSMA IN PROSTATE CANCER: RADIO-PHARMACEUTICAL BACKGROUND AND CLINICAL IMPLICATIONS. *Curr. Radiopharm.* **2017**, *11*, 4.
- (25) Grubmueller, B.; Baltzer, P.; D'Andrea, D.; Korn, S.; Haug, A. R.; Hacker, M.; Grubmueller, K. H.; Goldner, G. M.; Wadsak, W.; Pfaff, S.; Babich, J.; Seitz, C.; Fajkovic, H.; Susani, M.; Mazal, P.; Kramer, G.; Shariat, S. F.; Hartenbach, M. 68Ga-PSMA 11 ligand PET imaging in patients with biochemical recurrence after radical prostatectomy - diagnostic performance and impact on therapeutic decision-making. *Eur. J. Nucl. Med. Mol. Imaging* **2018**, *45* (2), 235–242.
- (26) Minamimoto, R.; Hancock, S.; Schneider, B.; Chin, F. T.; Jamali, M.; Loening, A.; Vasanaawala, S.; Gambhir, S. S.; Iagaru, A. Pilot comparison of 68Ga-RM2 PET and 68Ga-PSMA-11 PET in patients with biochemically recurrent prostate cancer. *J. Nucl. Med.* **2016**, *57* (4), 557–562.
- (27) Pyka, T.; Weirich, G.; Einspieler, I.; Maurer, T.; Theisen, J.; Hatzichristodoulou, G.; Schwamborn, K.; Schwaiger, M.; Eiber, M. 68Ga-PSMA-HBED-CC PET for differential diagnosis of suggestive lung lesions in patients with prostate cancer. *J. Nucl. Med.* **2016**, *57* (3), 367–371.
- (28) Rahbar, K.; Weckesser, M.; Huss, S.; Semjonow, A.; Breyholz, H.-J.; Schrader, A. J.; Schaefer, M.; Boegemann, M. Correlation of intraprostatic tumor extent with 68Ga-PSMA distribution in patients with prostate cancer. *J. Nucl. Med.* **2016**, *57* (4), 563–567.
- (29) Seitz, A. K.; Rauscher, I.; Haller, B.; Kroenke, M.; Luther, S.; Heck, M. M.; Horn, T.; Gschwend, J. E.; Schwaiger, M.; Eiber, M.; Maurer, T. Preliminary results on response assessment using 68Ga-HBED-CC-PSMA PET/CT in patients with metastatic prostate cancer undergoing docetaxel chemotherapy. *Eur. J. Nucl. Med. Mol. Imaging* **2018**, *45*, 602.
- (30) Breeman, W. A.; de Jong, M.; de Blois, E.; Bernard, B. F.; Konijnenberg, M.; Krenning, E. P. Radiolabelling DOTA-peptides with 68Ga. *Eur. J. Nucl. Med. Mol. Imaging* **2005**, *32* (4), 478–85.
- (31) Molinspiration Cheminformatics. 2017 Calculation of Molecular Properties and Bioactivity Score. <http://www.molinspiration.com/services/logp.html>.
- (32) Molinspiration Cheminformatics. LogP value calculation for Ga-68-WL12. <http://www.molinspiration.com/cgi-bin/properties>.
- (33) National Institute of Standards. Experimental logP and Molinspiration calculated logP for some industrial chemicals. <https://www.nist.gov/fusion-search?s+=Molinspiration&op=>.
- (34) Rolleman, E. J.; Valkema, R.; de Jong, M.; Kooij, P. P.; Krenning, E. P. Safe and effective inhibition of renal uptake of radiolabelled octreotide by a combination of lysine and arginine. *Eur. J. Nucl. Med. Mol. Imaging* **2003**, *30* (1), 9–15.
- (35) Donnelly, D. J.; Smith, R. A.; Morin, P.; Lipovsek, D.; Gokemeijer, J.; Cohen, D.; Lafont, V.; Tran, T.; Cole, E. L.; Wright, M.; Kim, J.; Pena, A.; Kukral, D.; Dischino, D. D.; Chow, P.; Gan, J.; Adelakun, O.; Wang, X. T.; Cao, K.; Leung, D.; Bonacorsi, S. J., Jr.; Hayes, W. Synthesis and Biologic Evaluation of a Novel (18)F-Labeled Adnectin as a PET Radioligand for Imaging PD-L1 Expression. *J. Nucl. Med.* **2018**, *59* (3), 529–535.